Physics Faculty Publications   Physics

Measurement of the Electric Form Factor of the Neutron at Q² = 0.5 and 1.0 GeV²/c²

Jefferson Lab E93-026 Collaboration

G. Warren

F. Wesselmann

H. Zhu

A. Klimenko
Old Dominion University

See next page for additional authors

Authors

Jefferson Lab E93-026 Collaboration, G. Warren, F. Wesselmann, H. Zhu, A. Klimenko, S. E. Kuhn, L. Yuan, J. Yun, B. Zihlmann, and et al.

Measurement of the Electric Form Factor of the Neutron at $Q^2 = 0.5$ and $1.0\ \mathrm{GeV}^2/c^2$

G. Warren,[1,2] F. Wesselmann,[3] H. Zhu,[3] P. McKee,[3] N. Savvinov,[4] M. Zeier,[3] A. Aghalaryan,[5] A. Ahmidouch,[6] H. Arenhövel,[7] R. Asaturyan,[5] I. Ben-Dayan,[8] F. Bloch,[1] W. Boeglin,[9] B. Boillat,[1] H. Breuer,[4] J. Brower,[10] C. Carasco,[1] M. Carl,[9] R. Carlini,[2] J. Cha,[11] N. Chant,[4] E. Christy,[12] L. Cole,[12] L. Coman,[9] M. Coman,[9] D. Crabb,[3] S. Danagoulian,[6] D. Day,[3] K. Duek,[8] J. Dunne,[11] M. Elaasar,[13] R. Ent,[2] J. Farrell,[3] R. Fatemi,[3] D. Fawcett,[3] H. Fenker,[2] T. Forest,[14] K. Garrow,[2] A. Gasparian,[12] I. Goussev,[1] P. Gueye,[12] M. Harvey,[12] M. Hauger,[1] R. Herrera,[9] B. Hu,[12] I. Jaegle,[1] M. Jones,[2] J. Jourdan,[1] C. Keith,[2] J. Kelly,[4] C. Keppel,[12] M. Khandaker,[15] A. Klein,[16] A. Klimenko,[16] L. Kramer,[9] B. Krusche,[1] S. Kuhn,[16] Y. Liang,[12] J. Lichtenstadt,[8] R. Lindgren,[3] J. Liu,[4] A. Lung,[2] D. Mack,[2] G. Maclachlan,[10] P. Markowitz,[9] D. McNulty,[3] D. Meekins,[2] J. Mitchell,[2] H. Mkrtchyan,[5] R. Nasseripour,[9] I. Niculescu,[2] K. Normand,[1] B. Norum,[3] A. Opper,[10] E. Piasetzky,[8] J. Pierce,[3] M. Pitt,[17] Y. Prok,[3] B. Raue,[9] J. Reinhold,[9] J. Roche,[2] D. Rohe,[1] O. Rondon,[3] D. Sacker,[1] B. Sawatzky,[3] M. Seely,[2] I. Sick,[1] N. Simicevic,[14] C. Smith,[3] G. Smith,[2] M. Steinacher,[1] S. Stepanyan,[5] J. Stout,[6] V. Tadevosyan,[5] S. Tajima,[18] L. Tang,[12] G. Testa,[1] R. Trojer,[1] B. Vlahovic,[19] B. Vulcan,[2] K. Wang,[3] S. Wells,[14] H. Woehrle,[1] S. Wood,[2] C. Yan,[2] Y. Yanay,[8] L. Yuan,[12] J. Yun,[17] and B. Zihlmann[20]

(Jefferson Lab E93-026 Collaboration)

[1]Universität Basel, CH-4056 Basel, Switzerland
[2]Thomas Jefferson National Accelerator Facility, Newport News, Virginia 23606, USA
[3]University of Virginia, Charlottesville 22903, USA
[4]University of Maryland, College Park, Maryland 20742, USA
[5]Yerevan Physics Institute, Yerevan, Armenia
[6]North Carolina A&T State University, Greensboro, North Carolina 27411, USA
[7]Johannes Gutenberg-Universität, D-55099 Mainz, Germany
[8]Tel Aviv University, Tel Aviv, 69978 Israel
[9]Florida International University, Miami, Florida 33199, USA
[10]Ohio University, Athens, Ohio 45071, USA
[11]Mississippi State University, Mississippi State, Mississipi 39762, USA
[12]Hampton University, Hampton, Virginia 23668, USA
[13]Southern University at New Orleans, New Orleans, Louisiana 70126, USA
[14]Louisiana Tech University, Ruston, Louisiana 71272, USA
[15]Norfolk State University, Norfolk, Virginia 23504, USA
[16]Old Dominion University, Norfolk, Virginia 23529, USA
[17]Virginia Polytechnic Institute & State University, Blacksburg, Virginia 24061, USA
[18]Duke University and TUNL, Durham, North Carolina 27708, USA
[19]North Carolina Central University, Durham, North Carolina 27707, USA
[20]Vrije Universiteit, 1081 HV Amsterdam, The Netherlands

The electric form factor of the neutron was determined from measurements of the $\vec{d}(\vec{e}, e'n)p$ reaction for quasielastic kinematics. Polarized electrons were scattered off a polarized deuterated ammonia ($^{15}\mathrm{ND}_3$) target in which the deuteron polarization was perpendicular to the momentum transfer. The scattered electrons were detected in a magnetic spectrometer in coincidence with neutrons in a large solid angle detector. We find $G_E^n = 0.0526 \pm 0.0033(\mathrm{stat}) \pm 0.0026(\mathrm{sys})$ and $0.0454 \pm 0.0054 \pm 0.0037$ at $Q^2 = 0.5$ and $1.0\ (\mathrm{GeV}/c)^2$, respectively.

The electric form factor of the neutron G_E^n is a fundamental quantity in nuclear physics. Knowledge of G_E^n over a large range of momentum transfer leads to insight to physics beyond the simple SU(6) symmetric models, for which it must vanish. Beyond nucleon structure, our understanding of G_E^n has an impact on a broad range of topics, which vary from the charge radii of nuclei [1] to extracting the strangeness content of the nucleon [2].

Historically, measurements of G_E^n have suffered from large uncertainties due to experimental technique and nuclear model dependence. Early attempts to measure G_E^n from cross sections sometimes failed to determine even the sign. Until recently, the best determination of G_E^n came from elastic electron-deuteron measurements, but the errors were large, $\sim 30\%$, due to their dependence on the nucleon-nucleon potential model [3]. The first

polarization measurements of G_E^n, conducted with ^{2}H and ^{3}He targets, differed significantly because final state interactions were not addressed [4,5]. These experiences highlight the importance of measuring G_E^n using different reactions.

In the past few years, the experimental understanding of G_E^n has improved considerably. The results from polarization experiments described in Refs. [6–11] are consistent and provide good accuracy in the kinematic region of the four-momentum transferred squared $Q^2 \leq 0.7$ (GeV/c)^2 [henceforth units of Q^2 are assumed to be (GeV/c)^2]. Until now, values of G_E^n determined from the deuteron quadrupole form factor [12] provide the only information in the kinematic region above $Q^2 \gtrsim 0.7$ and leave the $Q^2 > 1.6$ region undetermined.

This Letter describes a first measurement of G_E^n at $Q^2 = 1.0$ using a polarized target. In addition, the result for $Q^2 = 0.5$ has half the uncertainty as the previous measurement [6] and is the most precise result near the peak of G_E^n. These results are largely insensitive to the model of the nucleon-nucleon (NN) potential so that, compared to those of Ref. [12], they are more reliable.

To determine G_E^n, the helicity dependent rate asymmetry in electron scattering was measured. In the ideal case of a polarized electron scattering elastically off a free polarized neutron, with the neutron polarization vector in the scattering plane and perpendicular to the momentum transfer $\vec{q}$, G_E^n is related to the beam-target asymmetry term A_{en}^V [13] by

$$A_{en}^V = \frac{-2\sqrt{\tau(\tau + 1)}\tan(\theta_e/2)G_E^n G_M^n}{(G_E^n)^2 + \tau[1 + 2(1 + \tau)\tan^2(\theta_e/2)](G_M^n)^2}, \quad (1)$$

where $\tau = Q^2/4M_n^2$, M_n is the mass of the neutron, G_M^n is the magnetic form factor of the neutron, and θ_e is the electron scattering angle.

For lack of a free neutron target, the actual measurements were performed on a polarized deuterium target. The measured experimental asymmetries were due to a combination of several physics asymmetries scaled by the electron and target vector and tensor polarizations (that are described in detail in our previous work [6], not repeated here for brevity's sake). The proper averaging of the asymmetry (symmetrically around $\vec{q}$) and the negligible contributions from the target tensor asymmetry simplify the relationship of the measured asymmetry ϵ to the deuteron vector asymmetry A_{ed}^V so that $\epsilon = fP_eP_1^dA_{ed}^V$, where P_e is the beam polarization, P_1^d is the deuteron vector polarization, and f is the dilution factor due to scattering from nucleons other than polarized deuterons in the target. Calculations show that A_{ed}^V depends linearly on G_E^n for the kinematics of the experiment [14].

The measurements were conducted in Hall C of the Thomas Jefferson National Accelerator Facility in a setup similar to that of the previous measurement [6]. The longitudinally polarized electron beam [15] was scattered off a polarized frozen deuterated ammonia (^{15}ND$_3$) target. The scattered electrons were detected by the high momentum spectrometer (HMS), and the neutrons were detected by a dedicated neutron detector. The central kinematics for the two measurements as well as the average beam and target polarizations are listed in Table I. The average deuteron luminosity was 10^{35} cm^2 s.

The polarized target [16] consisted of ammonia granules submerged in liquid He and maintained at 1 K by a ^{4}He evaporation refrigerator. The target spins were aligned by a 5 T magnetic field generated by a pair of superconducting coils. The polarization was enhanced via dynamic nuclear polarization [17] and measured with a continuous-wave NMR system [18]. To minimize localized heating and depolarization of the target material, the electron beam was rastered uniformly in a circular pattern with a 1 cm radius.

A two-magnet chicane compensated for the deflection of the electron beam by the target field. After traversing the target, the beam passed through a helium bag to a special dump in the experimental hall. The polarization of the beam was measured at regular intervals throughout the experiment with a Møller polarimeter [19]. The beam helicity was changed in a pseudorandom sequence 30 times per second to minimize charge fluctuations correlated with helicity.

The HMS was operated in its standard mode for the detection of electrons. The established reconstruction algorithms were augmented to account for the large beam rastering and the effects of the target magnetic field on the scattered electrons.

The neutron detector consisted of multiple vertical planes of segmented plastic scintillators. Two planes of thin scintillators served to distinguish charged particles. Behind these were six planes of thick scintillators to detect the neutrons. All scintillators were equipped with photomultipliers on both ends to provide spatial and time information for the detected particle. The 88 thick scintillators provided a neutron detection volume that was roughly 160 cm wide, 160 cm tall, and 90 cm deep. The front of the detection volume was approximately 4.2 m and 6.2 m from the target during the $Q^2 = 0.5$ and 1.0 measurements, respectively. The detector was shielded

TABLE I. Central kinematics and average polarizations. E (E') is the energy of the incident (scattered) electron. θ_e (θ_n) is the angle of the scattered electron (neutron). θ_B is the orientation of the target polarization axis. $\langle P_e \rangle$ and $\langle P_t \rangle$ are the average beam and target polarizations, respectively.

Q^2 (GeV/c)^2	E (GeV)	E' (GeV)	θ_e (deg)	θ_n (deg)	θ_B (deg)	$\langle P_e \rangle$ (%)	$\langle P_t \rangle$ (%)
0.5	2.331	1.963	-18.5	60.5	150.4	78.2	24.1
1.0	3.481	2.810	-18.0	53.3	143.3	71.8	23.8

from direct gamma rays from the target by a 2.5 cm lead curtain, and the entire assembly was housed in a thick-walled concrete hut, which was open to the target.

The trigger was set up so that the neutron detector was read out for every electron trigger in the HMS. Coincidences between the electrons and the knockout nucleon were determined off-line.

The experiment was simulated using Monte Carlo (MC) techniques. The simulation package, based on MCEEP [20], included the charged particle transport through the target's magnetic field and the optical and aperture model of the HMS from the Hall C simulation package SIMC [21]. The MC served two principal functions: to determine the dilution factor and to average the theoretical asymmetries over the acceptance. For the dilution factor, all target materials were included in the simulation: the deuterium and the nitrogen in the ammonia, the liquid helium bath, the aluminum target cell windows, and the NMR coil.

Contributions from electron-neutron events originating from quasielastic scattering and pion production were included in the MC for all target materials. It was found that the $(e, e'n)\pi$ contribution to the event sample was negligible for $Q^2 = 0.5$ and less than 0.5% for $Q^2 = 1.0$. Two-body knockout contributions were examined in the MC (following [22]) and were also negligible.

The simulated rates were normalized to the measured ammonia rates, and the variations in the ratios of MC rate to observed rate for various target materials were used to determine the uncertainty in the dilution factor. A comparison of event distributions of the data and MC for several kinematic variables for $Q^2 = 1.0$ is shown in Fig. 1; agreement is very good. The comparison for the $Q^2 = 0.5$ data is similar and slightly better than in the previous experiment [6].

Several corrections to the measured asymmetry were applied. The leading correction was for charge exchange of protons in the lead shielding: $-3.8 \pm 1.1\%$ ($-3.3 \pm 3.0\%$) for $Q^2 = 0.5$ ($Q^2 = 1.0$). The charge exchange in the target material itself was small: $-0.3 \pm 0.3\%$ ($-0.3 \pm 0.3\%$). The accidental background rate was $1.9 \pm 0.1\%$ ($0.5 \pm 0.2\%$) with no statistically significant asymmetry. Internal radiation effects on the asymmetry were also corrected: $0.9 \pm 0.5\%$ ($0.6 \pm 0.5\%$). The effect of external radiation was insignificant compared to the 0.5% MC statistical uncertainty. The contamination from neutral pions generated by protons in the lead shielding of the neutron detector was also found to be insignificant.

The physics model of A_{ed}^V used in the MC was based on the calculations of Arenhövel, Leidemann, and Tomusiak [14]. It included a nonrelativistic description of the $n - p$ system in the deuteron using the Bonn R-space NN potential [23] for both the bound state and the final state interactions. The full calculation included meson exchange, isobar configuration currents, and relativistic corrections.
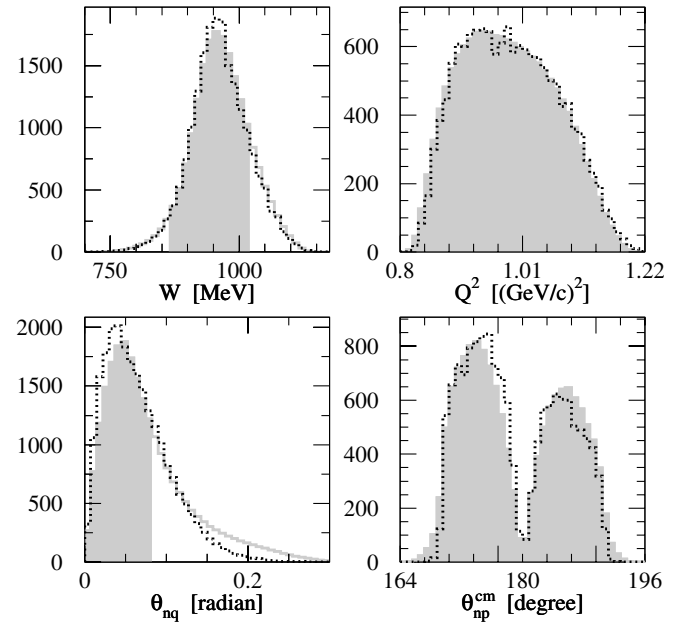

FIG. 1. Comparison of $Q^2 = 1.0$ MC and data electron-neutron event distributions from all materials in the target for four kinematic variables: invariant mass W, Q^2, angle between the neutron and $\vec{q}$ in lab frame θ_{nq}, and angle between neutron-proton system and the momentum transfer in the center-of-momentum frame θ_{np}^{cm}. The solid grey histograms correspond to the data, and the dotted black histograms correspond to the simulation. Only the shaded regions, dominated by events from ^{2}H were used to determine G_E^n.

The model assumed a scaled Galster parametrization [24] for G_E^n and the dipole parametrization for G_M^n. The Galster parametrization is $G_E^n(Q^2) = -\mu_n\tau/(1 + 5.6\tau)G_D(Q^2)$, where $G_D = 1/(1 + Q^2/0.71)^2$ is the dipole form factor. Various scale factors of this parametrization, ranging from 0.5 to 1.5, were examined. The potential impact of the Q^2 dependence of the G_E^n parametrization was found to be negligible because the Q^2 acceptance was not large and the Q^2 dependence of G_E^n over the acceptance was mostly linear. The acceptance-averaged value of A_{ed}^V has a linear dependence on G_M^n, so one can trivially correct for more accurate G_M^n values.

The value of G_E^n was determined by comparing the acceptance averaged A_{ed}^V of the data to that of the MC. The theoretical asymmetries were determined for a range of scaling factors of the Galster parametrization to determine the corresponding G_E^n: G_E^n/Galster $= 1.003 \pm 0.064$ and 1.172 ± 0.140 for $Q^2 = 0.5$ and 1.0, respectively. The uncertainties are statistical only. To account for the slight deviations of G_M^n from the dipole form factor, the recent fit to the G_M^n data [25] was used: $G_M^n/\mu_n G_D = 1.007 \pm 0.005$ and 1.072 ± 0.014 for $Q^2 = 0.5$ and 1.0, respectively. Then the values for G_E^n are

$$G_E^n(Q^2 = 0.5) = 0.0526 \pm 0.0033 \pm 0.0026,$$
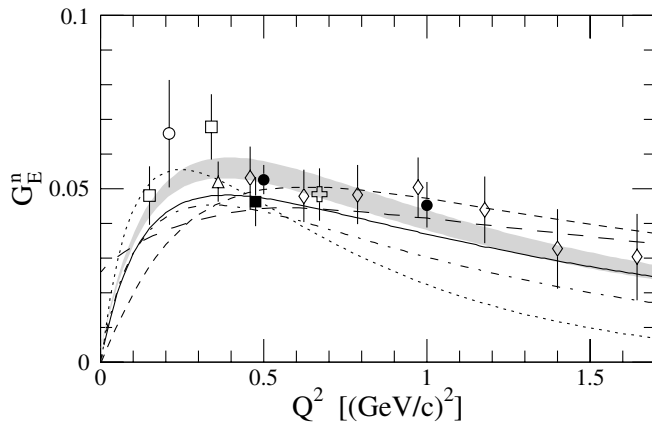$$G_E^n(Q^2 = 1.0) = 0.0454 \pm 0.0054 \pm 0.0037, \quad (2)$$

FIG. 2. Comparison of this experiment with data from recent measurements. The data points are diamonds [12], hollow squares [10], triangle [4], hollow circle [7], solid square [6], and plus sign [11]. Solid circles: This Letter. See text for a description of the curves.

where the first uncertainty is statistical and the second is systematic. The $Q^2 = 0.5$ result agrees well with the previous result reported in Ref. [6].

Other systematic uncertainties for $Q^2 = 0.5$ ($Q^2 = 1.0$) were dilution factor 3.4% (3.0%), target polarization 2.9% (4.6%), central kinematic values 1.2% (3.4%), and beam polarization 1.1% (3.3%).

The results as compared to recent measurements are shown in Fig. 2. The new data at $Q^2 = 1.0$ provides the important experimental confirmation of the decline of G_E^n following the Galster form. The data shown in the figure were fit to the form $G_E^n(Q^2) = -\mu_n a\tau/(1 + p\tau)G_D(Q^2)$. The parameter $a = 0.895 \pm 0.039$, the slope at $Q^2 = 0$, is fixed by atomic measurements of the neutron charge radius [26]. The fit yielded $p = 3.69 \pm 0.40$. The errors obtained for the fit parameters are uncorrelated. The one-sigma error region of the fit is shown in Fig. 2 as the shaded band.

Many recent models [27–31] have attempted to predict or fit the nucleon electromagnetic form factors. Figure 2 compares the data with two recent calculations that use covariant formulations of the constituent quark model with quark-quark interactions fitted to spectroscopic data. The pointform spectator approximation (PFSA) of [30] (dot-dashed line) uses a Goldstone boson exchange interaction with pointlike constituent quarks while the light-front (LF) calculation of [28] (short-dashed line) uses a one-gluon exchange interaction with constituent quark form factors fitted to data for $Q^2 < 1$. The use of constituent form factors improves the fit to the nucleon magnetic form factors at larger Q^2, but the PFSA seems to describe G_E^n better at low Q^2 with fewer parameters.

Also shown in Fig. 2 are the results from a hybrid model that interpolates between vector-meson dominance at low Q^2 and perturbative QCD at high Q^2 [27] (solid line), from a light-front model where the nucleon is considered a system of three bound quarks surrounded by a cloud of pions [31] (long dashed line) and from a soliton model [29] (dotted line) whose basic features include an extended object, partial coupling to the vector mesons, and relativistic recoil corrections. While all these models agree qualitatively with the data, none agree with the data for the entire range of Q^2.

It is remarkable that, in the past five years, the experimental precision in G_E^n measurements has improved to the 10% level. This significant improvement provides a rigorous challenge for models of the nucleon structure because this electromagnetic form factor is the most sensitive to physics beyond the simplistic SU(6) symmetric picture.

In conclusion, the electric form factor of the neutron at $Q^2 = 0.5$ and 1.0 has been determined from measurements of the beam-target asymmetry. This experiment provides the highest Q^2 measurement to date using a polarized target and the most precise measurement near the maximum of G_E^n.

[1] J. L. Friar and J.W. Negele, Adv. Nucl. Phys. **8**, 219 (1975).
[2] K. S. Kumar and P. A. Souder, Prog. Part. Nucl. Phys. **45**, S333 (2000).
[3] S. Platchkov *et al.*, Nucl. Phys. **A510**, 740 (1990).
[4] J. Becker *et al.*, Eur. Phys. J. A **6**, 329 (1999).
[5] M. Ostrick *et al.*, Phys. Rev. Lett. **83**, 276 (1999).
[6] H. Zhu *et al.*, Phys. Rev. Lett. **87**, 081801 (2001).
[7] I. Passchier *et al.*, Phys. Rev. Lett. **82**, 4988 (1999).
[8] J. Golak *et al.*, Phys. Rev. C **63**, 034006 (2001).
[9] T. Eden *et al.*, Phys. Rev. C **50**, R1749 (1994).
[10] C. Herberg *et al.*, Eur. Phys. J. A **5**, 131 (1999).
[11] J. Bermuth *et al.*, Phys. Lett. B **564**, 199 (2003); D. Rohe *et al.*, Phys. Rev. Lett. **83**, 4257 (1999).
[12] R. Schiavilla and I. Sick, Phys. Rev. C **64**, 041002(R) (2002).
[13] T.W. Donnelly and A. S. Raskin, Ann. Phys. (N.Y.) **169**, 247 (1986); A. S. Raskin and T.W. Donnelly, Ann. Phys. (N.Y.) **191**, 78 (1989).
[14] H. Arenhövel, W. Leidemann, and E. L. Tomusiak, Z. Phys A **331**, 123 (1988); **334**, 363(E) (1989); H. Arenhövel, W. Leidemann, and E. L. Tomusiak, Phys. Rev. C **46**, 455 (1992); H. Arenhövel (unpublished).
[15] C. Sinclair, TJNAF Report No. TJNAF-TN-97-021.

[16] D. Crabb and D. Day, Nucl. Instrum. Methods Phys. Res., Sect. A **356**, 9 (1995); T. D. Averett *et al.* Nucl. Instrum. Methods Phys. Res., Sect. A **427**, 440 (1999).

[17] D. G. Crabb and W. Meyer, Annu. Rev. Nucl. Part. Sci. **47**, 67 (1997).

[18] G. Court, Nucl. Instrum. Methods Phys. Res., Sect. A **324**, 433 (1993).

[19] M. Hauger *et al.*, Nucl. Instrum. Methods Phys. Res., Sect. A **462**, 382 (2001).

[20] P. Ulmer, MCEEP: Monte Carlo for Electro-Nuclear Coincidence Experiments, Version 3.5.

[21] J. Arrington, SIMC.

[22] S. Janssen, J. Ryckebusch, W. Van Nespen, and D. Debruyne, Nucl. Phys. A **672**, 285 (2000).

[23] R. Machleidt, K. Holinde, and Ch. Elster, Phys. Rep. **149**, 1 (1987).

[24] S. Galster *et al.*, Nucl. Phys. **B32**, 221 (1971).

[25] G. Kubon *et al.*, Phys. Lett. B **524**, 26 (2002).

[26] S. Kopecky *et al.*, Phys. Rev. Lett. **74**, 2427 (1995).

[27] E. L. Lomon, Phys. Rev. C **66**, 045501 (2002).

[28] F. Cardarelli and S. Simula, Phys. Rev. C **62**, 065201 (2000); Phys. Lett. B **467**, 1 (1999).

[29] G. Holzwarth, hep-ph/020138; Z. Phys. A **356**, 339 (1996) (Fit B2 is shown in Fig. 2).

[30] S. Boffi, L. Ya. Glozman, W. Klink, W. Plessas, M. Radici, and R. F. Wagenbrunn, Eur. Phys. J. A **14**, 17 (2002).

[31] G. A. Miller, Phys. Rev. C **66**, 032201(R) (2002).